Chapter 6

# Rotational Components of the Seismic Fields Caused by Local Events

Anna Kurzych, Krzysztof P. Teisseyre,
Zbigniew Krajewski and Leszek R. Jaroszewicz

Additional information is available at the end of the chapter

http://dx.doi.org/10.5772/59595

## 1. Introduction

The existence of rotation effects at the Earth surface associated with earthquakes has been observed probably at least from the times when scientific approach to the ground motions during the quake had started. They are described in several classical monographs, such as Hobbs [1] and Davison [2], in which cited examples concern, among other things, twisting of some obelisks, tombs and segments of columns. However, early publications explain such phenomena as incidental effects of interference between linear vibrations [3, 4]. For instance, Imamura [5] explained the rotation effects of some objects at the ground surface by the impact of body/surface waves: due to such impact, an object can be inclined, partly losing contact with the ground surface, and when returning to the vertical some twist occurs with respect to its former position. Hence, from the beginning, the rotational effects have been treated as derivative effects, and it was stated that although such effects are observed, they cannot be explained as effect of any rotational waves - or rotational components of seismic waves - because existence of such waves or components would contradict the ideal elastic theory [6].

In the second half of last century, it was observed a spectacular development of continuum mechanics including defects, granular structure and other deviations from the ideal linear elasticity. Special interests were concentrated on the micropolar and micromorphic continua. In such elastic continua, the real rotation can be accompanied by other kind of axial motion – the twist-bend motion. On above base, it was theoretically proved that so-called the seismic rotation waves could propagate through grained rocks, initially by Teisseyre [7] who initially attributed the appearance of rotation components in seismic wave by coupling the seismic waves with the micromorphic response of the medium characterized by the an internal/ granular structure [7, 8]. From this time, this possibility was extended to rocks with micro-

structure or defects [9, 10] or even without any internal structure [11 -13], due to the asymmetric stresses in the medium. On this base, various types of rotational waves have been discussed theoretically [14, 15].

It should be stressed that seismologists share different opinions about the nature of rotation waves – see the preface of a monograph on rotational seismology [16]. Perhaps, as it is underlined in preface of a book [16], still the majority believes that such rotation motions are not related to inner rotations but are directly related to rotation in the displacement field which may reach much higher magnitudes in materials with an internal structure than in homogenous layers; considering damages in the high buildings, there are many examples indicating enormous increase of rotation effect caused by consecutive impacts of seismic body and surface waves.

Nevertheless, all above aspects can be treated as elements of rotational seismology. It is an emerging field for studying all aspects of rotational ground motions induced by earthquakes, explosions, an ambient vibrations. It should be noticed that nowadays there is observed rapid growth of the rotational seismology interest in many geophysical fields of knowledge [17] which includes wide seismology disciplines, seismological apparatus, seismic-origin phenomena, physical and engineering aspects of earthquakes as well as geodesy.

However practical aspect of rotational events and phenomena investigation is connected with method of their recording, and different rotational seismology branches need different devices. For example, earthquake physics need devices operating with sensitivity below $10^{-9}$ rad/s/$Hz^{1/2}$, whereas the engineering of a strong-motion seismology devices operating with a frequency range 0.05-100 Hz with sensitivity $10^{-6}$-$10^{-1}$ rad/s/$Hz^{1/2}$ [18]. In this subject, it should be noticed that the seismic rotation waves were for the first time effectively recorded in Poland in 1976 [19]. Even though, from this time, waves or phenomena of this type have been studied in a few centers over the world, a further experimental verification of the existing rotational phenomena needs a new approach to the construction of the measuring devices, because the conventional seismometers are inertial sensors detecting only linear velocities [20]. Thus, during measurement of the rotation present in the seismic field, with the use of a special array or set of conventional seismometers (for example based on a set of two classical mechanical seismometers [21]), data are disturbed by linear movements [22]. Therefore, an innovative device is necessary to detect the rotational seismic phenomena/events. According to our knowledge we can confirm that the technical implementation of the Saganc effect [23] is the most proper way to measure rotation directly. One can find instances of such solution: a ring laser [24] as well as a fibre optic seismometer [25-27]. It gives the opportunity to carry out the measurements without any reference system.

It should be underlined that all experimental data recorded during earthquakes shows that rotational components are small in comparison to linear motions - less than 10% [14, 19] or have half of above value and exist with some delay regarding last one [25].

Based on above review in this chapter we present an analysis of a few examples of the rotational seismograms. Authors have concentrated on the local seismic events obtained at the Książ Observatory in Poland. These signals were obtained from two kinds of sensors described in

http://dx.doi.org/10.5772/59595

section 2: the micro-array of TAPSs – Twin Antiparallel Pendulum Seismometers (also named rotation seismometers or double pendulum horizontal electromagnetic seismometers) and with the Sagnac interferometer of AFORS - Autonomous Fibre-Optic Rotational Seismometer, constructed at the Institute of Geophysics and the Military University of Technology, respectively. It should be also underlined that signals derived from micro-array include two components which, according to Asymmetric Continuum Theory, have character of rotational wave: rotation $\omega$ and shear $E$ (called also pure shear) – see [14]. On the other side, the Sagnac-type seismometers detect only rotation and are completely insensitive to translations [25, 28, 29] which may contaminate rotational measurements. Nevertheless, probably all the signals analyzed here suffer from some disturbances, this is referred to in the section 3.

## 2. Instrumentation for recording rotational components of the seismic events

Figure 1 presents the general view of the measurement devices installed, at the beginning of July 2010, in the Książ Observatory, Poland (located at 50.84380333N, 16.291755 E). There are AFORS-1, the micro-array of seismometers consisting of two TAPSs (TAPS-1 and TAPS-2) oriented perpendicularly in the N-S and E-W directions, and other instruments such as accelerometers (parallel positioned with TAPSs), etc.

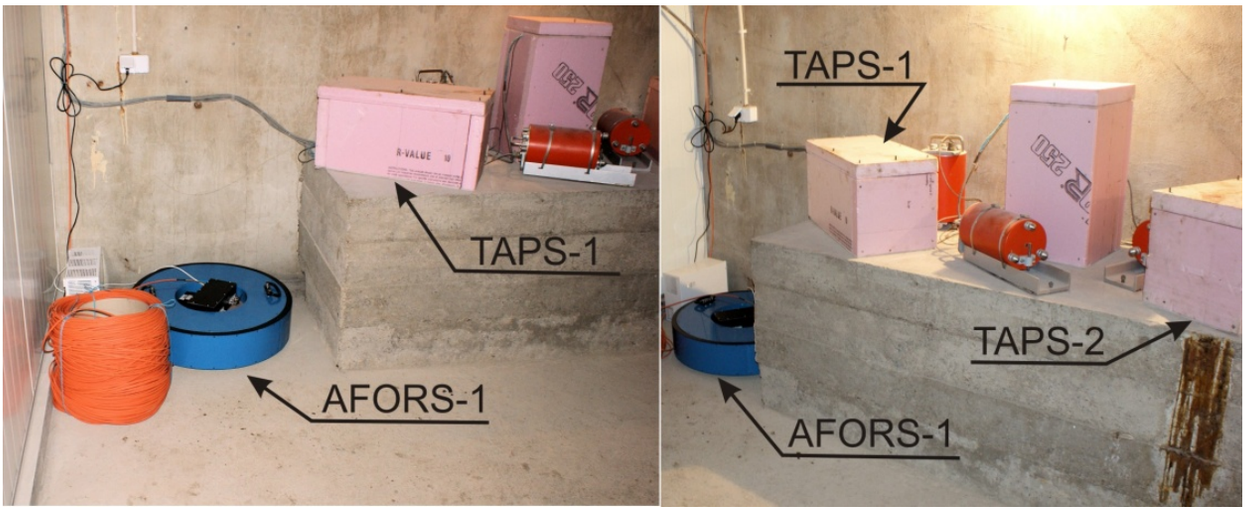


**Figure 1.** The general view of measurement devices installed in the Książ Observatory

The data detected by TAPSs (two channels for each of them) are stored by standard seismological system KST while data detected by AFORS are stored both by FORS-Telemetric Server and KST. The KST system uses sampling of the signals with frequency equals 12,8 kHz. The process of data storing by KST uses frequency of 100 Hz. Figure 2 presents an example of a diagram with data collected on March 11$^{th}$, 2011 at 6 h 58 min. (after the Honshu earthquake

M=9.0 on March 11th, 2011 at 5 h 46 min. 23 s UT, recorded in Książ, Poland on March 11th, 2011 at 5 h 58 min. 35 s UT), used in previously presented analysis [30].

### 2.1. Design of the Twin Antiparallel Pendulum Seismometers

The micro-array of seismometers (system of two TAPSs perpendicularly oriented) is an experimental apparatus, devised in the Institute of Geophysics, and manufactured according to description presented below, on the base of short period SM-3 seismometers. This is one of the simplest micro-arrays for measuring the rotation and twist (shear) [14]. It was deployed at two Polish observatories, in Książ and Ojców (see [31]). The third identical set of sensors was used in Central Italy [32].

The idea of using the classical short period SM-3 seismometer as a new kind of mechanical rotational seismometer named TAPS is presented in Figure 3 [21]. It is a set of two SM-3 seismometers (named in Figure 3b as left – L and right – R) situated on a common axis and connected in parallel, but with opposite orientation. In the case of the ground motion containing displacements $w(t)$ and rotation $\alpha(t)$, the $u$(t) - electromotive force recorded by each simple seismometer contains a component of displacement ($\pm w$) and rotation motion ($\alpha$) multiplied by a proper length of pendulum ($l$) [33]:

$$u(t)_{L,\,R} = \pm w\left(t\right) + l \cdot \alpha(t), \tag{1}$$

where sign "+" and "-" are for R and L seismometer, respectively.

As one can see, in the case of identical two seismometers the rotational motions and displacement can be obtained from the sum and difference of the two recorded signals as:

$$\begin{aligned} \alpha(t) &= [u(t)_R + u(t)_L]/2l, \quad \text{a} \\ w\left(t\right) &= [u(t)_R - u(t)_L]/2l. \quad \text{b} \end{aligned} \tag{2}$$

If the ground could be treated as a perfect rigid body, then the rotational motion recorded by sole one TAPS was identical to rotation. But rocks and the ground surface are not perfectly rigid; they transfer the mechanical waves due to slight, transient deformations which, seen along different axes, may different. Consequently, rotation $\omega$ in the plane of measurements and the given moment are calculated as a mean of rotational motions received at one and the other TAPS, while the twist $E$ (pure shear) is obtained as half of their difference:

$$\begin{aligned} \omega(t) &= [\alpha_1(t) + \alpha_2(t)]/2, \quad \text{a} \\ E(t) &= [\alpha_1(t) - \alpha_2(t)]/2. \quad \text{b} \end{aligned} \tag{3}$$

Relations (2a) and (2b) remain valid, however, only when both seismometers forming the system have exactly the same response characteristics. Because, as a matter of fact, the

http://dx.doi.org/10.5772/59595

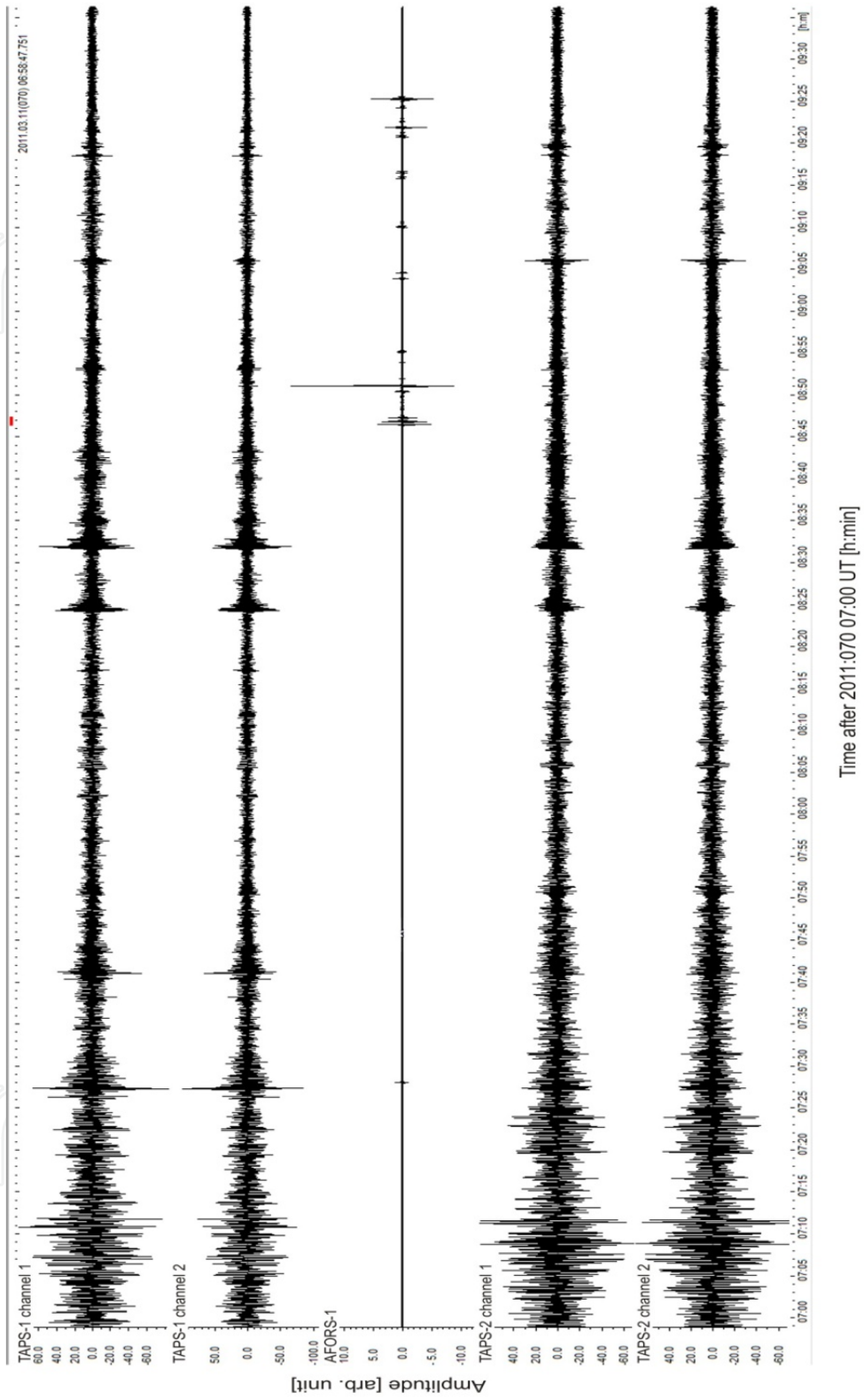


**Figure 2.** Plots of the seismic events recorded in the Książ Observatory, Poland on March 11th, 2011 starting from 06:58 UT, after the Honshu M=9.0 earthquake [30]

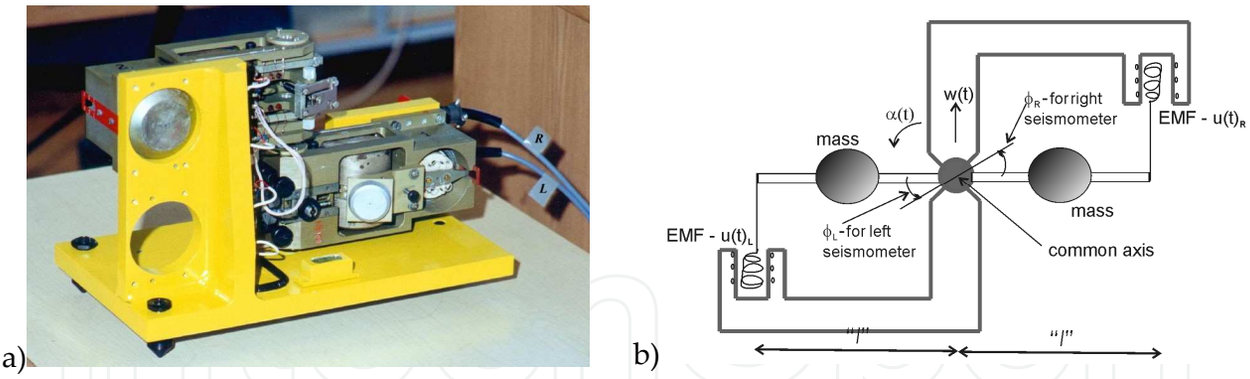


**Figure 3.** The TAPS – Twin Antiparallel Pendulum Seismometer: a) general view, b) schematic view

pendulum seismometers are, inevitably, slightly different, the special TAPS channels calibration algorithm is used. In this system, for the aim of comparing both sensors, it is possible to rotate the position of one seismometer in such a way that both the pendulum seismometers, suspended on the common axis become oriented in the same directions, one just above the other – this is the test position. The working and test position for the case of the horizontal seismometers are schematically shown in Figure 4. The records obtained in the test positions can differ mainly due to differences in their response characteristics, and to minimize these errors, the following left channel signal calibration procedure is usually applied:

$$u_L^{'} = u_L \sqrt{\sum u_R \cdot u_R / \sum u_L \cdot u_L}\,, \tag{4}$$

where: $u_L$ and $u_R$ are electromotive forces recorded by left and right seismometers in test position.

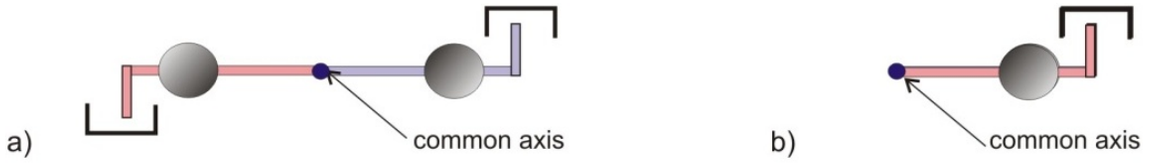


**Figure 4.** The TAPS: working a) and calibration b) positions of the pendulum seismometers

Nevertheless, there is some discrepancies due to the recording procedure in the case of the present of the difference of TAPS' pendulums attenuation characteristics. Figure 5 presents the simulation which indicates that there can be some errors in the data caused by the recording proceeding. The considered simulation was made for the attenuation difference equals $|\beta_L - \beta_R| = 0.05$ between left and right seismometer attenuation. It is easy to see that the major error of the signal is present when the simulated rotation is characterized by smaller value of amplitude compared to the simulated translation component. However, this is the region where the seismic-origin rotation is expected. For above reason the process of TASP calibration seems to

http://dx.doi.org/10.5772/59595

be an essential complication of the system work's correctness. Moreover, the extremely high sensitivity to the translational motions of the seismometers (preferred for the component of displacement detection) taken into account in their construction can limit the accuracy of such devices, too.

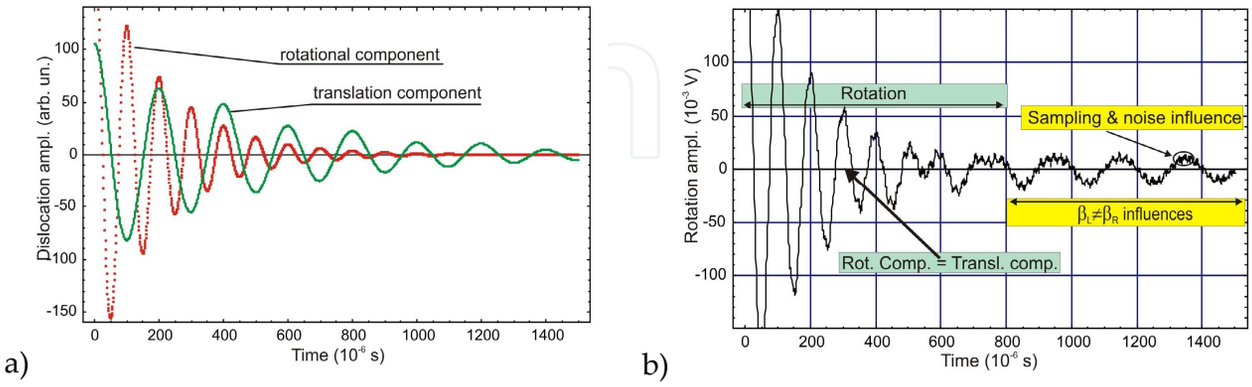


**Figure 5.** The simulated displacement and rotational components of the seismic event - a) and rotational signal detection by the TAPS - b) [22]

From above mentioned reasons, the additional numerical procedures for improving the TAPS performance may be applied, based on filtering in frequency [34] or in time [35] domains. The respective filters can then be applied to records in the normal working position to reduce the influences of non-equal operation of pendulum seismometers, presented above. However, these methods use test position of the TAPS, that generally changes the condition of the TAPS operation. For this reason, another procedure of the recorded data processing, based on smoothing by the spline functions has been also proposed [36]. It should be noticed, that the main disadvantage of all listed methods is that they operate on recorded data, which can limit TAPS usefulness for some applications. In the research presented in this paper, the mentioned methods of signal correction were not used.

## 2.2. Design of the Autonomous Fibre-Optic Rotational Seismograph

The AFORS-1, used in our research, is one of three such devices existing in Poland and manufactured on the base of fibre-optic gyroscope, all dedicated for direct measurement of rotational components existing in seismic events and having accuracy below $5 \cdot 10^{-9}$ rad/s for 1 Hz detection band.

The physical principle for these devices is the Sagnac effect [23] which is a result of difference between two beams propagating around closed optical path, in opposite direction. Figure 6a presents the basic principle of the Sagnac's experiment. The input light beam is splitted by a beam splitter into a beam circulating in the loop in a clockwise - cw direction (Figure 6a - beam T) and a beam circulating in the same loop in a counterclockwise - ccw direction (Figure 6a – beam R). One can observe the interference pattern, in the output light, caused by the interference phenomenon of the two waves. In the case of the present of rotation with an angular rate

represented by vector $\vec{\Omega}$ rad/s then a fringe shift $\Delta Z$ is observed in the output of the interferometer. The fringe shift is given by the formula [23]:

$$\Delta Z = \vec{\Omega} \bullet \vec{S} / (\lambda_0 \cdot c), \tag{5}$$

in which $\vec{s}$ is a vector of sensor loop area, $\lambda_0$ is the wavelength of the used light in vacuum, c is velocity of light in vacuum. According to the above formula a fringe shift is proportional to the cosine of angle between the axis of rotation and the normal to the sensor plane. There have been used the indigo mercury wavelength as well as the sensor area S = 866cm$^2$ in the Sagnac's experiment [23] which gave the fringe shift equals 0.07 fringes for the rotational speed equal to 2 rps. Nevertheless other papers [37] indicate that the possible detectable fringe shift was of the order of 0.01 fringe in those time. Thus, perhaps Sagnac has been carried out the research with a maximal accuracy. Sagnac also established that the effect does not depend on the shape of surface area S or on the location of the centre of rotation, whereas future investigation shown that this effect it does not depend on the presence of a commoving refracting medium in the path of the beam [37].

Figure 6b presents the Sagnac interferometer in the optical fibre solution which uses optical waveguide of the long length L wound on sensor loop of the diameter D which was shown firstly in 1976 [38]. In this approach, a phase shift $\Delta\phi$ is produced between cw and ccw propagating light, given by:

$$\Delta\phi = \frac{2\pi \cdot L \cdot D}{\lambda_0 \cdot c}\Omega, \tag{6}$$

where $\Omega$ is the rotational component perpendicular to the sensor loop. It is clearly to indicate that the sensitivity can be change by physical dimension of the sensor loop as well as by the length of the applied waveguide. It should be noticed that application of three such systems, which loops are jointly perpendicular, provides data about space vector of the rotation. One can obtain the position change in space by integrating the data in time domain. The above procedure is used in the configuration of the fibre optical gyroscope - FOG which now, nearly 40-years from 1976, is the best recognized interferometric sensor performed in the fibre-optic technology.

However, for a desired rotation rate in the range of $10^{-6}$ – $10^{-9}$ rad/s, the Sagnac effect generates a very small phase shift, so it is needful to separate and protect this effect from other disturbances so that the Sagnac effect is the unique nonreciprocal effect in the device. For this reason all FOGs use, shown in Figure 7, the reciprocal configuration [39] which is also called minimum gyro-configuration [40]. This configuration guarantees an ideal equilibrium of two counter-propagating beams in the interferometer by obtaining true single mode operation at the common input-output port of the system. It is not disturbed even by non-single mode operation in the another part of the interferometer.

http://dx.doi.org/10.5772/59595

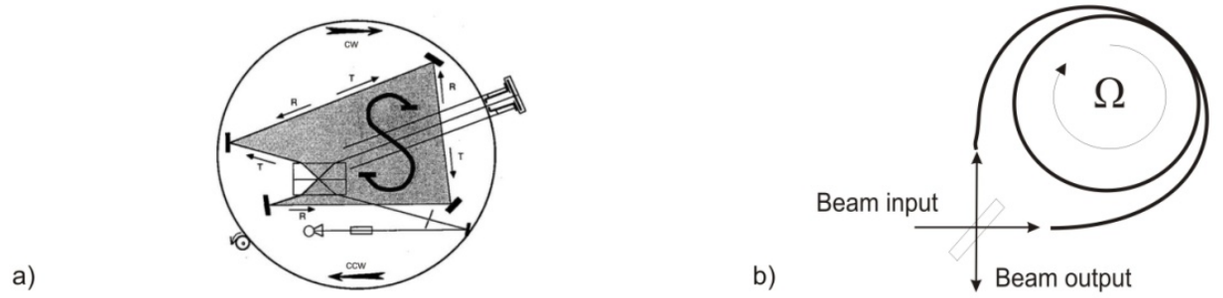


**Figure 6.** Schematic of the original Sagnac's experiment a) and its implementation in fibre optic technique b)

It is well known that each interferometric devices yield a cosine response. For above reason the detected signal practically do not change during the small changes of the rotation due to slow changes of the cosine function at the zero. In order to obtain higher sensitivity the operation point of the interferometer is shifted by applied additional phase shift modulation. The FOG utilizes the reciprocal phase modulator which is placed in the end of the sensor loop. It caused the modulation of the phase shift by propagation delay without any residual zero offset [41]. In this way one obtain the odd response instead of even one. An ultimate performance is, however, obtained only if the unbiased response is perfectly even and the biasing modulation has only odd frequencies. Therefore, the applied phase modulator is also a delay line filter operating at the eigen-frequency [42] – the delay in the loop is equal to a half of modulation period which suppresses the residual even harmonic signals. Nowadays the FOG utilizes broad-band light source for eliminating the Kerr effect which produces the phase shift in the optical fiber Sagnac interferometer [43]. Such a broadband source is also needed to remove coherence related with noise and drift due to backscattering and backreflection as well as lack of rejection of the polarizer [44–46]. Finally, for achieving the high scale factor linearization, FOG uses a digital phase step feedback [47] by the same reciprocal phase modulator as the biasing modulator and all-digital processing procedures where demodulation is carried by a digital subtracting and sampling of the modulated signal is obtained by using analogue-digital converter [48, 49].

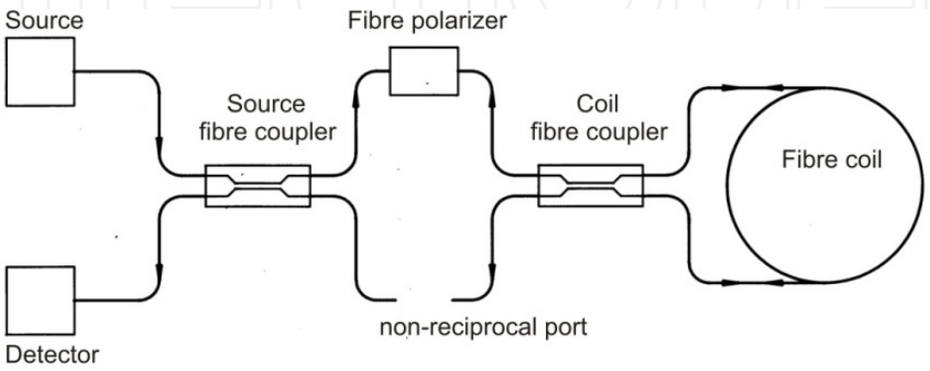


**Figure 7.** The minimum configuration of the FOG [39]

Currently, a digital processing of FOG systems is designed to record angular changes instead of rotation rates, thus, the optimization of such system to register the interesting phenomena from the rotational seismology point of view is problematic. Therefore it should be emphasized that the AFORS construction based on experiences according to the FOG development described above, but with system optimization for a direct measurement of the rotation rate only [22]. Such an approach gives a system which through a direct use of the Sagnac effect can limit drift influence on a device operation.

A detailed description of the AFORS system was published previously [29, 30, 50], hence here we summarized the above data regarding AFORS-1 construction, calibration and management. The second device - AFORS-2 is located in Warsaw (Poland) for initial works connected to the investigation of the irregular engineering construction torsional response and the interstory drift [51]. We anticipate that the new device, based on AFORS-1 and -2, AFORS-3 will be construed in the 2014 which gives us the opportunity to mount new innovative system instead of FORS-II assembled in seismological observatory Ojców, Poland [52].

The AFORS uses the minimum configuration of the FOG, however opposite of it, AFORS operates in open-loop architecture with digital data processing [53]. This technical solution is motivated by the fact that rotation events (Ω) are registered as sudden changes of rotational rate which amplitude is determined in a direct way from the Sagnac phase shift (Δφ) by following equation [37]:

$$\Omega = S_o \cdot \Delta\phi = \frac{\lambda \cdot c}{2\pi \cdot D \cdot L} \cdot \Delta\phi \tag{7}$$

where $S_0$ is the optical constant of interferometer which depends on the fundamental parameters of fibre coil.

Upper part of Figure 8 presents the block diagram of the AFORS-1 optical part configuration. The AFORS-1 construction, designed according to the minimum-gyro configuration, contains of the: SLED diode (ΔB=31.2 nm, $\lambda_0$ = 1305.7 nm, $P_{out}$= 9.43 mW; *Exalos*, Switzerland), isolator ($\alpha$=0.34 dB, 39 dB isolation; *FCA*, Poland), depolarizator (DOP<5%, $\alpha$=0.20 dB; *Phoenix Photonics*, UK), two mounted-in-line polarizators (ε=43 dB, $\alpha$=0.45 dB each; *Phoenix Photonics*, UK), two X-couplers ($\alpha$=0.20 dB; *Phoenix Photonics*, UK), sensor loop, phase modulator (*Piezomechanik GmbH*, Germany) and detector (S=0.9 A/W; *Optoway Technology Inc.*, Taiwan). The SLED diode has been chosen for two reasons. Firstly, SLED diode is the broad-band light source, which minimalizes the disadvantageous polarization as well as coherence effects [54, 55]. Additionally, this diode gives an opportunity to obtain a high optical power, which has a direct influence on the system sensitivity. In order to isolate the diode from the backscattering we applied the optical fibre isolator. To ensure truly depolarized light the depolarizer is used before the polarizers which guarantee the single mode operation in the entirely system as well as fulfil function of the filter. Two couplers ensure that both propagating waves have the same optical path. The detector's system consists of a PIN diode and a preamplifier. The sensor loop has been made by winding 15 000 m of the SMF-28e+ length on a special composite material

http://dx.doi.org/10.5772/59595

which includes permalloy particles for shielding the system from external magnetic field. The double-quadrupole method of winding [56] was used in order to stabilize the work system during the temperature fluctuation. The technical optimization of AFORS-1 construction (optical fibre of 15 000 m with attenuation equals 0.451 dB/km in 0.63 m sensor loop) allows to obtain a theoretical sensitivity equal to $1.97 \cdot 10^{-9}$ rad/s/Hz$^{1/2}$ in quantum noise limitation.

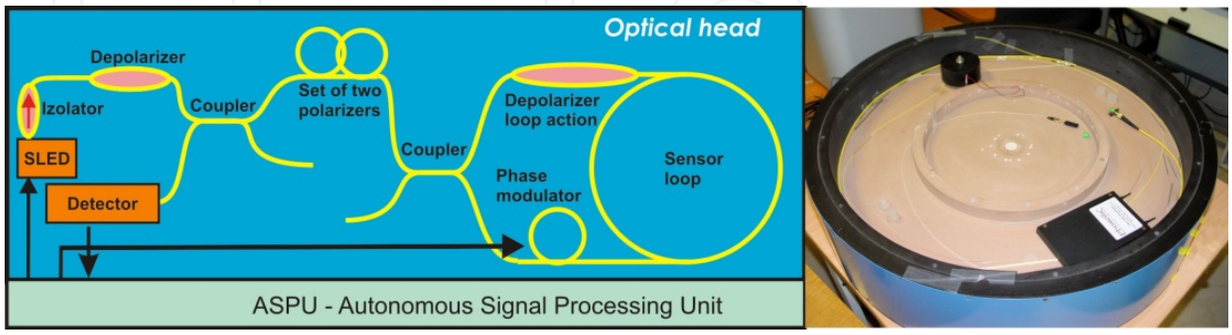


**Figure 8.** General schema and view of the AFORS optical head (generation of the Sagnac phase shift proportional to the measured rotation rate)

It should be emphasised that in the AFORS construction we have applied the special processing unit ASPU (Figure 9), which enables to obtain the detected rate of rotation in a direct way from the measured Sagnac phase shift (7). The ASPU detects the rotation rate ($\Omega$) by selection and conversion of the first ($A_{1\omega}$) and second ($A_{2\omega}$) amplitude of the harmonic output signal [u(t)] using the following formula [50]:

$$\Omega = S_o \cdot \arctan[S_e \cdot u(t)] = S_o \cdot \arctan[S_e \cdot \frac{A_{1\omega}}{A_{2\omega}}], \tag{8}$$

in which $S_e$ is the electrical constant connected to specification of the used instrumentations and received by calibrating the sensor, while $S_o$ is the optical constant determined also during the calibration process which is described below. In order to eliminate a discontinuity the formula (8) uses the arc tangent which is extended to the four quarters ($-\pi$, $\pi$) after the Fourier transform. The ASPU utilizes the synchronous detection in a digital form. The 32 bit digital signal processor realizes all necessary processing processes including calculation the rate of rotation in a real time as well as data recording in the SD card. The electronic part sends also the stored data via fibre patch cord to the GSM/GPS modem which is connected FORS-Telemetric Server [30, 50]. The fundamental time constant equals 4.7104 ms and its value resulted from the used quartz oscillator. The multiplication (maximum multiplication is equal to $2^7$) of the time constant allows to adjust the sampling time. This approach gives detection frequency bandpass from 0.83 Hz to 106.15 Hz. This detection band is required to detect the rotational seismic-origin events. Furthermore the electronic part is equipped with digital-to-analogue converter which enable to store the data in the analogue form by the standard recording system KST.

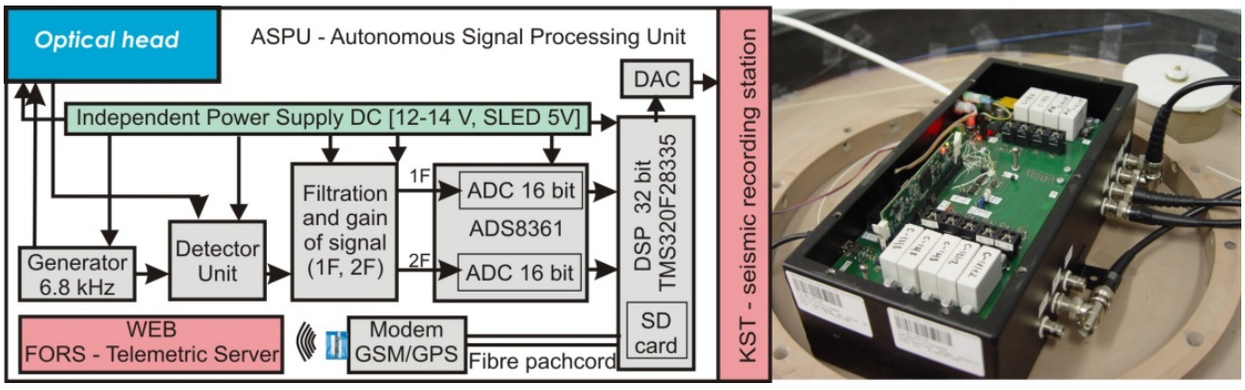


**Figure 9.** General schema and view of the AFORS's Autonomous Signal Processing Unit (rotation calculation and recording)

The calibration process was realized basing on the measurement of the defined slow rotation connected to the vector of Earth rotation in Warsaw, Poland (i.e. $\Omega_E$= 9.18 deg/h ≡ 4.45•10$^{-5}$rad/s for $\phi$ = 52°20′′). AFORS was mounted vertically on a special rotation table (Figure 10a) and then rotated so that the sensor loop was directed to the North, South, East and West. The detected signal was equalled to zero for East-West (sensor loop collinear with the Earth rotation axis) while the signal was maximal, equal to ± 4.45•10$^{-5}$rad/s, for North-South (the sensor loop perpendicular to the vector component of Earth rotation). During the calibration procedure in the first step were determined the position for maximal signals, North and South, then, the position of the sensor for the West and East was defined as the midpoint between those two signals because of problems with determination this position basing on searching of signals equal zero. The maximal signals were obtained with accuracy equals 0.5 deg. In order to eliminate the drift phenomenon the 10 night hours averaging signal was applied. The above procedure allows for scaling the system and determining the constant operation parameters – optical $S_o$ and electrical $S_e$. For AFORS-1 the following values of the above constants were obtained: $S_0$ = 0.043 s$^{-1}$, $S_e$ = 0.0144. In order to experimental determination of the accuracy for particular device [50], which have been made according to AFORS production technology, we measured the noise level for each of them. Nevertheless the measurements were carried out at Military University of Technology, Warsaw, Poland. The place of the research could provide deviations due to urban noises. The received accuracy is equal to 5.07·10$^{-9}$ rad/s and 5.51·10$^{-8}$ rad/s, respectively, for the lower and higher working detection frequency band, as shown in Figure 10b. Additional Figure 10b shows also measured parameters for second system - AFORS-2 (theoretical sensitivity in quantum noise limitation equals 2.46·10$^{-9}$ rad/s/Hz$^{1/2}$, accuracy in detection band at level of 4.81·10$^{-9}$ rad/s and 6.11·10$^{-8}$ rad/s). It should be noted that the linear dependence of AFORSs accuracy on the detection frequency band is an advantage of this system.

http://dx.doi.org/10.5772/59595

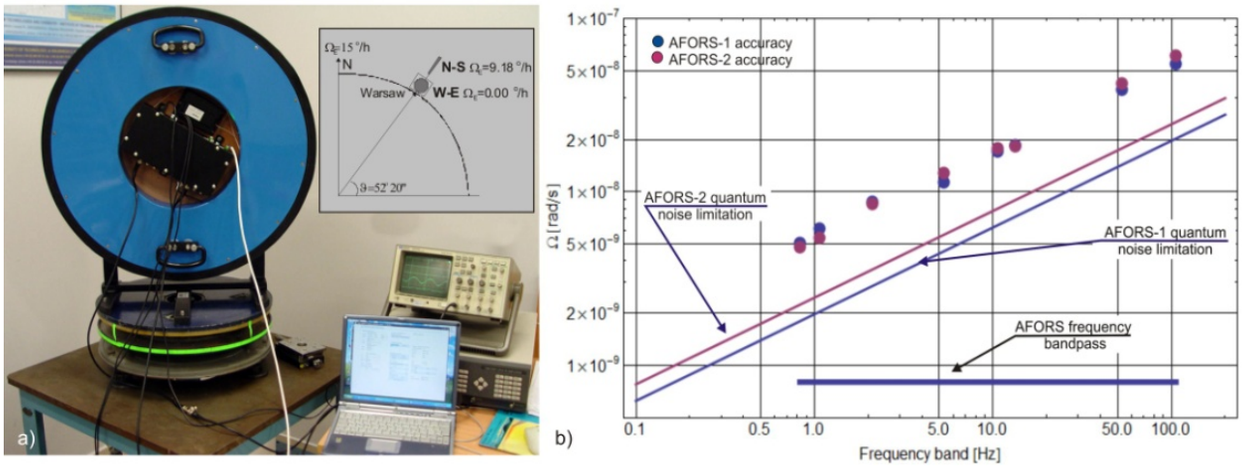


**Figure 10.** The calibration and investigation of AFORSs accuracies: a) general view of AFORS-1 during the calibration process with scheme showing its idea, b) the accuracy measured for the chosen detection frequency band for AFORS-1 and AFORS-2

## 3. Analysis of rotational components of the seismic fields caused by local events

In this section we present analysis of data obtained at Książ Observatory, reveal the rotational components presence in entire seismograms (from P-wave arrival onwards), for the cases of local seismic events, of the mining (Lubin on January 20th, 2011, two events starting at 04 h 59 min. 1 s UT - shown below as Figure 11) and tectonic (Jarocin on January 6th, 2012, the event starting at 15 h 38 min. 10 s UT - shown below as Figure 12) provenience.

The results were obtained directly from KST recording system and they include five plots: channels 1 and 2 for TAPS-1; channel 3 for AFORS-1; channels 4 and 5 for TAPS-2. The TAPSs' records show linear motions that appeared during the earthquakes, and rotational components are calculated as described in the section 2.1. The channel 3 for AFORS-1 shows rotational oscillations measured in a direct way.

As one can see, the both kinds of devices (AFORS-1 as well as set of micro-array of TAPSs) recorded the events in the same time, which can confirm some correlation between devices. However the following investigation needs an additional data proceedings. To limit noise influence on recorded signals the average procedure in the beginning has been applied. From above mentioned reason the recorded seismic events have been averaged in moving windows of 100 samples (which is equal to period of 1 second).

The results of above operation are presented in Figures 13a-13c respectively for above three events. Consistently, we present five plots for all of them. The first plot, named TAPS-1 channel 2, presents the velocity of linear ground motion in m/s registered by second seismometer in this device. Second diagram shows channel 1 of TAPS-2. It should be noticed that second channel for any TAPS, after change of sign, has very similar plot to the first channel, so they

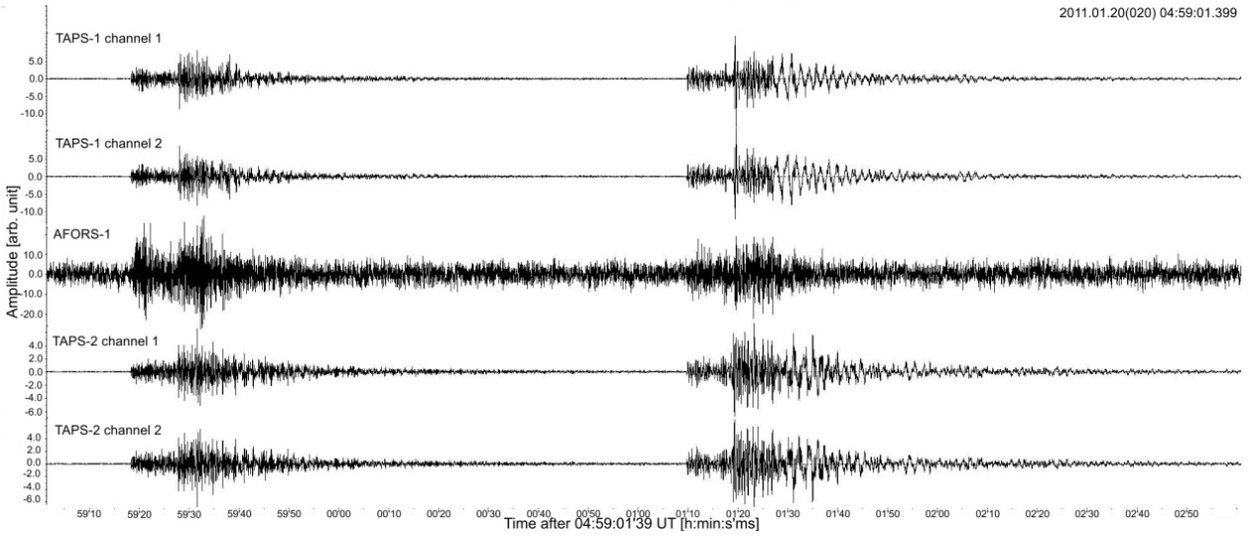


**Figure 11.** Plots of two seismic events with source in Lubin area: TAPS – ground motion velocity, AFORS – ground motion rotation rate

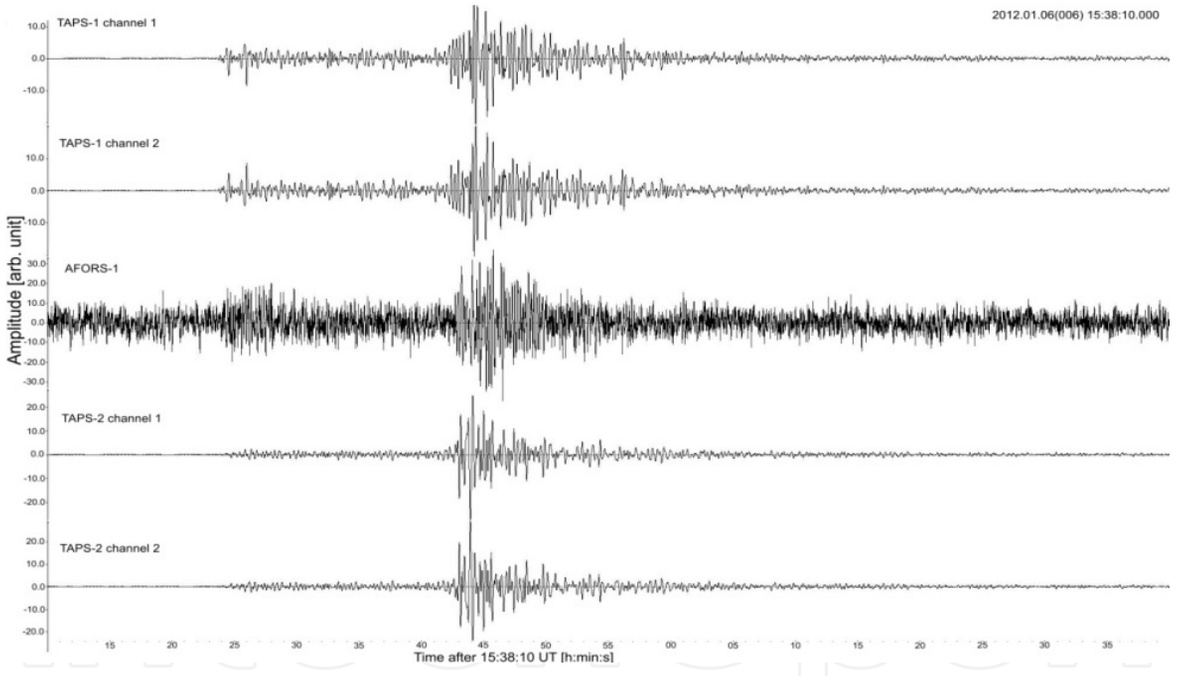


**Figure 12.** Plots of the seismic event with source in Jarocin area: TAPS – ground motion velocity, AFORS – ground motion rotation rate

are not presented both in our Figures. Third plot, named AFORS, presents the rotation velocity in rad/s, registered directly by AFORS-1. The result of measurement of the same component, but using the four simultaneous signals from micro-array of TAPSs (the procedure is described in section 2.1), is presented as plot four named Rotation from TAPS. Finally, last plot named Twist from TAPS, presents twist component obtained from the same micro-array in accord with, mentioned in the introduction, the Asymmetric Continuum Theory [14] – also in rad/s.

http://dx.doi.org/10.5772/59595

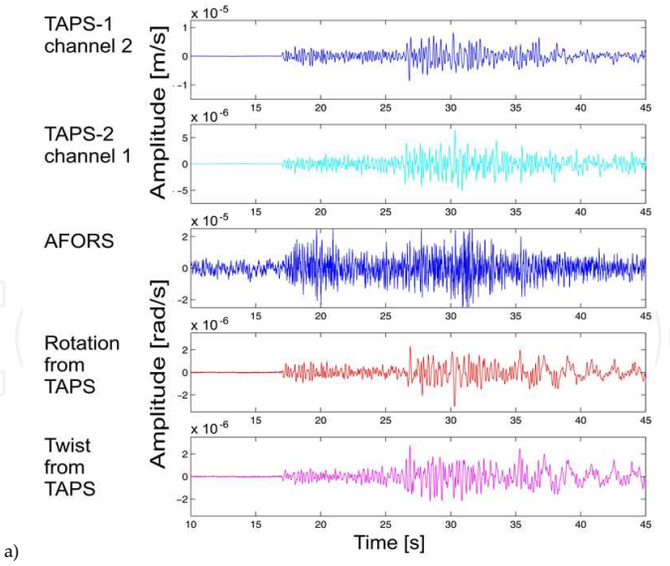


a)

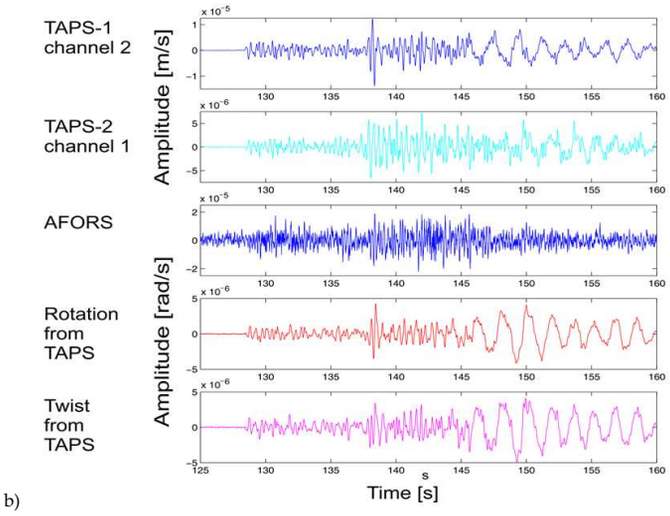


b)

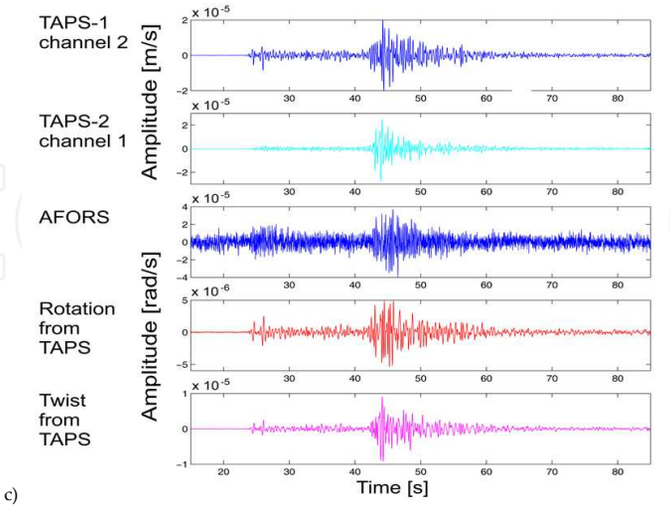


c)

**Figure 13.** (a). Results for the first event in the Lubin area registered on January 20th, 2011; (b). Results for the second event in the Lubin area registered on January 20th, 2011; (c). Results for the Jarocin area earthquake registered on January 6th, 2012

Even though the results presented in Figures 13a-13c show similar time of occurrence of the rotational components recorded by the AFORS-1 and calculated from TAPSs, their shape differs, and inevitably the correlation coefficients between them are low (though greater than zero). These coefficients are presented in Table 1, for both events recorded on January 20th, 2011, and for their selected parts. This selection consists of: time-period when P waves arrive – 2 seconds in each case; time period of firsts S waves arrivals – again 2 seconds, and a time-period when great S-type oscillations dominate; here we choose twenty seconds in each case (such unusually high amplitudes of low frequency oscillations, dominating in the late stage of the tremor, characterize the seismic field generated by mining seismic events in the Lubin area and received at Książ observatory).

| **20.01.2011.** | **First event 04 h 59 min., M=3.1** | | | **Second event 05 h 01 min., M=3.3** | | |
|---|---|---|---|---|---|---|
| **Lubin** | **17 – 107.75 s** | | | **128.40 – 234.45 s** | | |
| AFORS – Rot TAPS | 0.092 | | | 0.063 | | |
| Twist TAPS – ROT TAPS | 0.600 | | | 0.894 | | |
| Wave type time-period | P 17.00 – 19.00 s | S 26.00 – 28.00 s | great S 30.00 – 50.00 s | P 128.40 – 130.40 s | S 137.50 – 139.50 s | great S 146.00 – 166.00 s |
| AFORS – Rot TAPS | 0.200 | 0.354 | 0.073 | 0.187 | 0.050 | 0.140 |
| Twist TAPS – Rot TAPS | 0.166 | 0.483 | 0.641 | 0.534 | 0.724 | 0.958 |

**Table 1.** The correlation coefficients

Additionally, correlation between both rotational components calculated from TAPSs recordings, that is – rotation and twist – was checked too, for the same chosen time-periods. This appeared generally high (especially in the second event), which confirms previous observations by KP. Teisseyre that in the recordings of seismic events made with a set of TAPSs, there usually occurs conformance between rotation and twist, either direct or reverse.

Dissimilarity between simultaneous rotation recordings obtained from AFORS and the micro-array of TAPSs may be explained by different characteristics of the used instruments or by certain errors or/and noise present in one or the other side of compared results, or in both. Here, there is dramatic difference in spectra (Figure 14), that of AFORS is always much longer. For the analyzed case of mining events, the spectrum of AFORS signal bears high amplitudes in the range of 2 – 8 Hz. Spectra of all the signals and rotational components obtained from TAPSs are short – they practically decrease to zero level at about 20 Hz – and bear sharp maximum at about 0.5 Hz, while the linear signals have also wide area of relatively high amplitudes in the range of 1 – 8 Hz. Moreover, the signals from AFORS bear high percentage of noise, probably of electronic provenience.

http://dx.doi.org/10.5772/59595

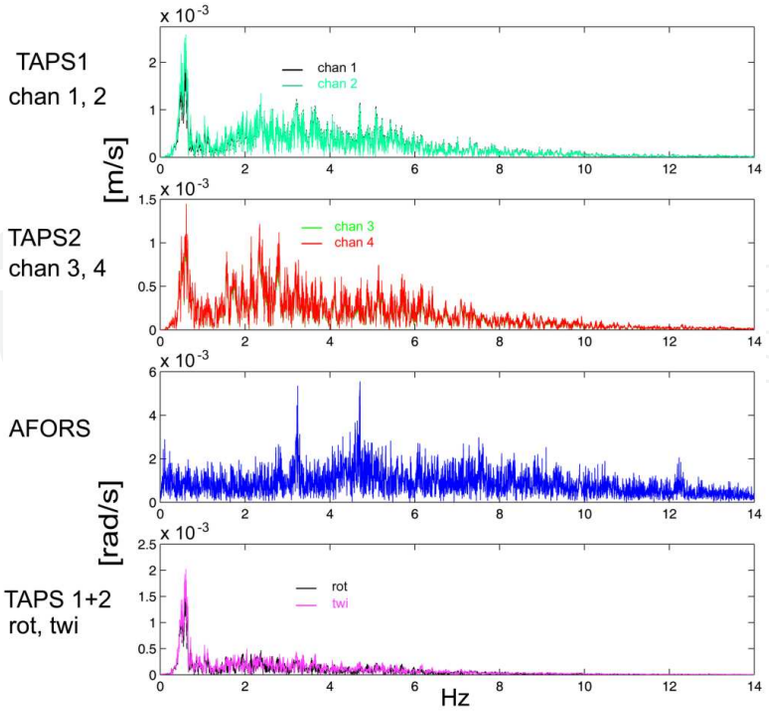


**Figure 14.** Spectra of linear and rotational signals, from ones of analysed seismic mining events, recorded on January 20th, 2011 at Książ observatory. The second one has the similar spectra

To find similarities in the obtained results in other way than just by sight, the following analysis has been applied. First – any of compared data chains was transformed into chain of absolute values (moduli). Then, the chains of moving averages of these moduli are created, with the window length of 100 samples, which is equivalent to 1 s. Here, absolute values of rotation (velocities) were compared – these from AFORS with those calculated from set of TAPSs. Further, analogical moving averages were investigated, but calculated from moduli of all four signals recorded by the TAPSs. If the rotation obtained from AFORS is symbolized with $\omega^o$, rotation obtained from the TAPSs with $\omega$, mean signal modulus from micro-array at the given sample with $\bar{u}$, and length of window used in moving average calculation with $w$, then formulae for described moving averages are as follows:

$$\bar{\omega}^{0} = \frac{\sum_{i=1}^{i=w} |\omega_i^0|}{w}, \quad \text{a}$$

$$\bar{\omega} = \frac{\sum_{i=1}^{i=w} |\omega_i|}{w}, \quad \text{b} \qquad (9)$$

$$\bar{u} = \frac{\sum_{i=1}^{i=w} \left( \frac{|u_1| + |u_2| + |u_3| + |u_4|}{4} \right)_i}{w}. \quad \text{c}$$

Results of this analysis are shown in Figures 15-17, which all have the same scheme. Diagrams a) show the plot of moving average of absolute values of the rotation rate obtained from AFORS; diagrams c) – analogical averages of rotation rate calculated from TAPSs' data; diagrams e) – analogical averages of the mean signals moduli from TAPSs – as in formula (9c). The blue plots presented in diagrams b) represent the moving correlation coefficient between moving averages of absolute rotation from AFORS and its analogue from TAPSs (compare the plots in diagrams a) and c) described mathematically by equations (9a) and (9b)). This coefficient is calculated for a window of 100 samples (1s). Additionally, in the same diagram we present reference thick lines – orange or mauve, and turquoise – which should facilitate the comparison of correlation coefficient with compared chains. The procedure for obtaining the upper reference line is following: create normalized chain (9b) to (9a) by comparing both maximum values, as (9b'). Next, make new chain as sum of (9a) with (9b'), and normalize it to 1. Thus we have obtained a doubly–normalized mean chain which joins shapes of the original two chains. The turquoise reference line is analogical to orange one, but multiplied by -1. Purpose of this line presence is to facilitate comparison of stages of high negative correlations between compared chains, again with the described doubly–normalized averages. Analogically, curves presented in diagrams d) and f) are the plots of the correlation coefficient in a moving window of 100 samples; in d) – between averages plotted in diagrams c) and e), and in f) – between averages plotted in e) and a). Reference lines are produced in analogical way as for diagrams b); the upper one is mauve in diagrams f). Figure 15 shows results of such analysis applied to recordings of first event from Lubin area; Figures 16 and 17 are made for second event from Lubin area and for Jarocin earthquake, in the same methodology.

Comparison of the moving correlation coefficients with the moving averages allows to find certain rule. In time-periods when main seismic phase arrive – as P and S (for local distances, it might be jointly for example Pg and Pb phases and analogically Sg and Sb in the S-type phases family), all investigated correlations between moving averages of the absolute signals are generally high. These are some of the time-periods in which blue line in the diagrams b), d) and f) is near 1, and the upper reference line rises. More interestingly, these time-periods starts slightly before any noticeable rise in initial moving averages, despite facts that all the moving windows had the same length. This phenomenon may have two causes: certain common order in concerned signals starts just before noticeable arrival of seismic waves, or/and this is a mere effect of filtration (which used in every contemporary seismic recording system).

The chosen time-periods of high correlations and rise of the moving averages are as follows.

For the first seismic event from Lubin - two time periods: from 16.2 to 18.5 s, this include arrival of P waves, and from 25.8 to 27 s, which include S waves arrival (see Table 1). For the second seismic event from Lubin – only one time period, from 127.9 to 129.5 s, which include arrival of P waves. For the Jarocin earthquake – one non-continuous time period, for diagrams b) and f): 21.7 – 24.1 s and for diagram d) : 20.9 – 24.1 s. This time-period, in all three diagrams, starts before arrival of P waves and comprises arrival of this seismic phase.

http://dx.doi.org/10.5772/59595

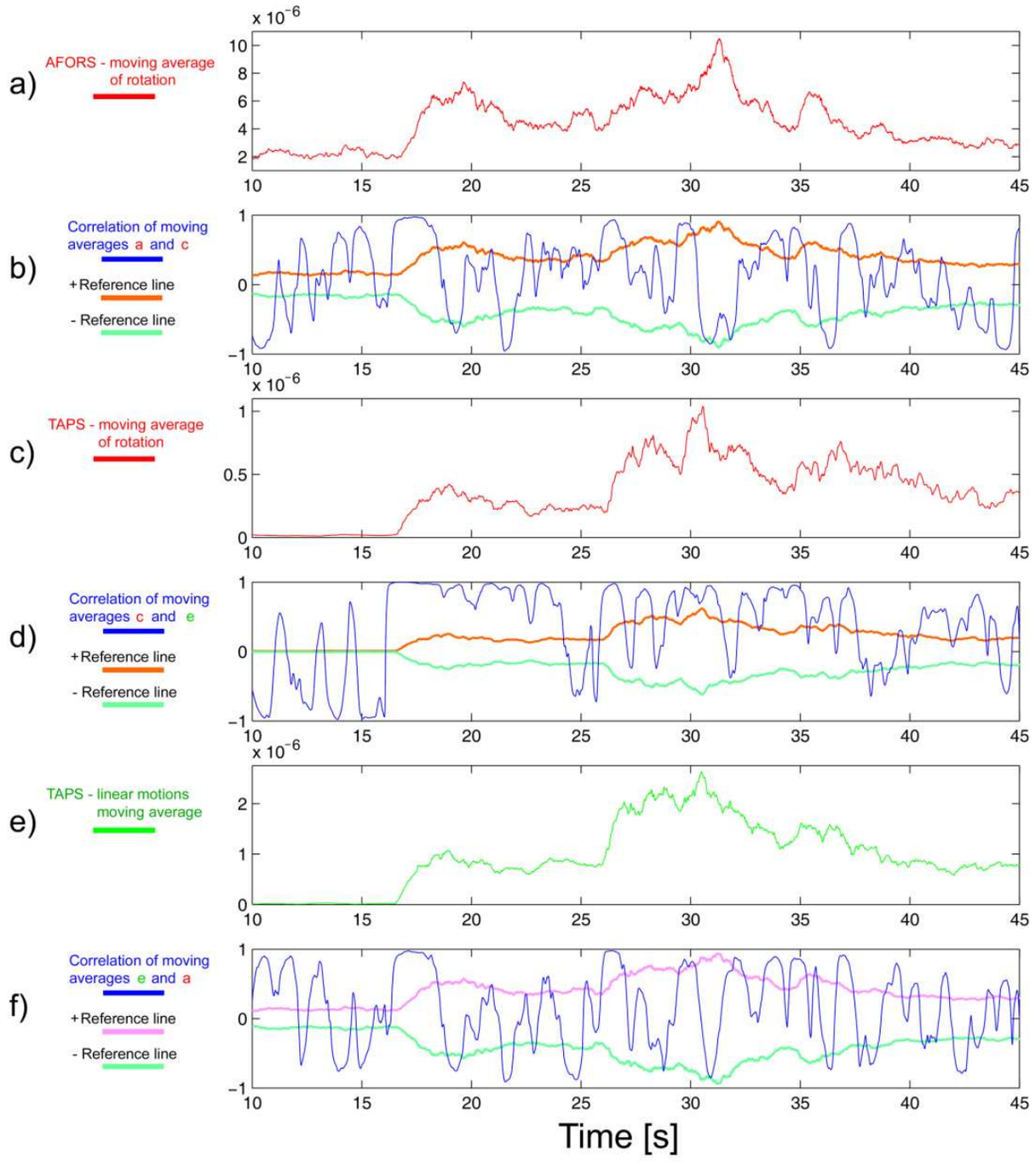


**Figure 15.** Relations of rotations and linear signals at the first event in Lubin area registered on January 20th, 2011. Diagrams: a) moving average of absolute values of AFORS – signal; b) correlation coefficient between (a) and (c) in moving window – blue line, orange reference line – doubly normalized means of (a) and (c), turquoise – the same as orange but with reversed sign; c) moving average of absolute values of rotations obtained from TAPSs; d) correlation coefficient between (c) and (e) in moving window, orange reference line – doubly normalized means of (c) and (e), turquoise – the same as orange but with reversed sign; e) moving average of absolute values of four channels of TAPSs; f) correlation coefficient between (e) and (a) in moving window, mauve reference line – doubly normalized means of (e) and (a), turquoise – the same as mauve but with reversed sign

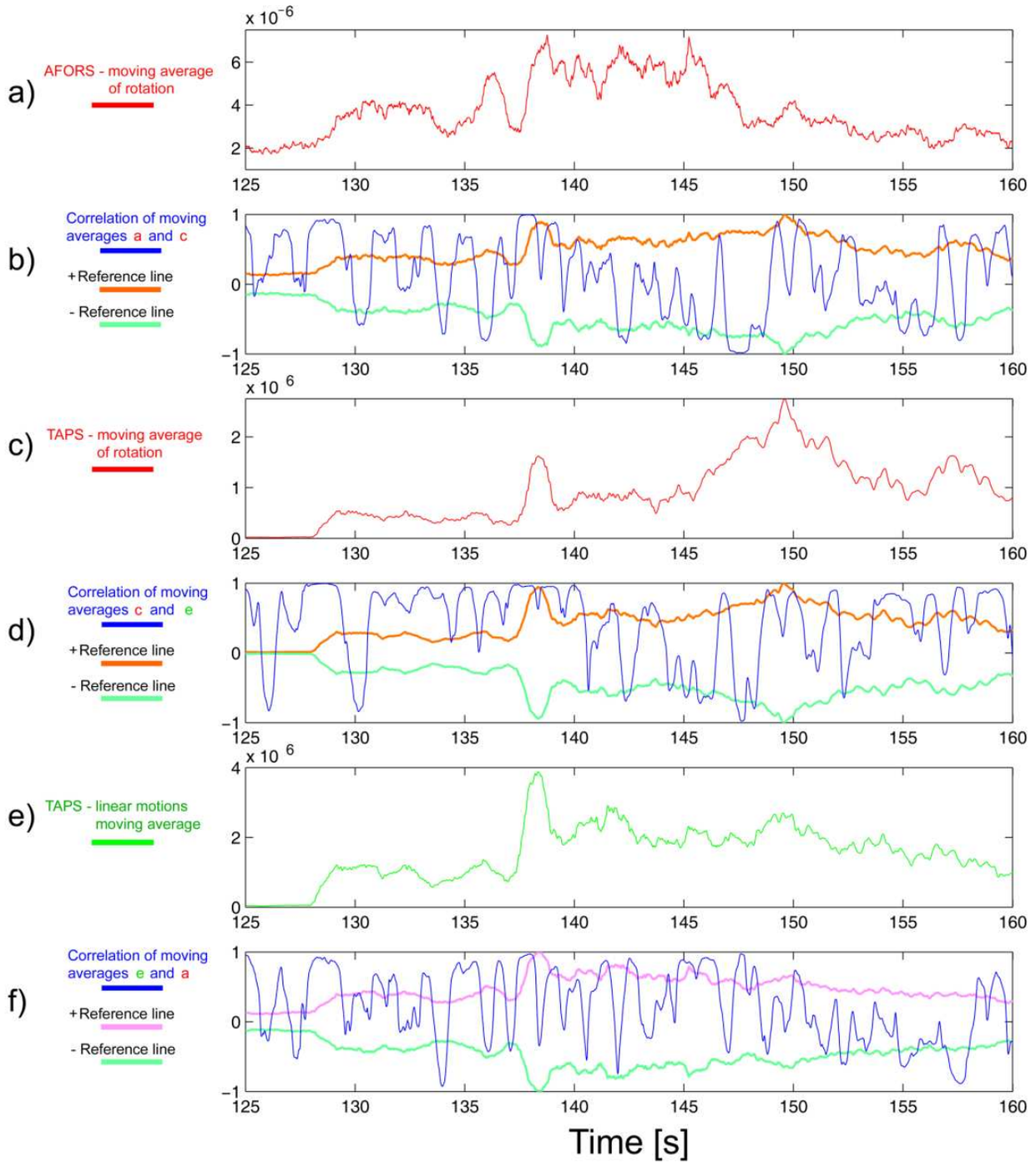


**Figure 16.** Relations of rotations and linear signals at the second event in Lubin area registered on January 20th, 2011. Diagrams descriptions as in Fig. 15

http://dx.doi.org/10.5772/59595

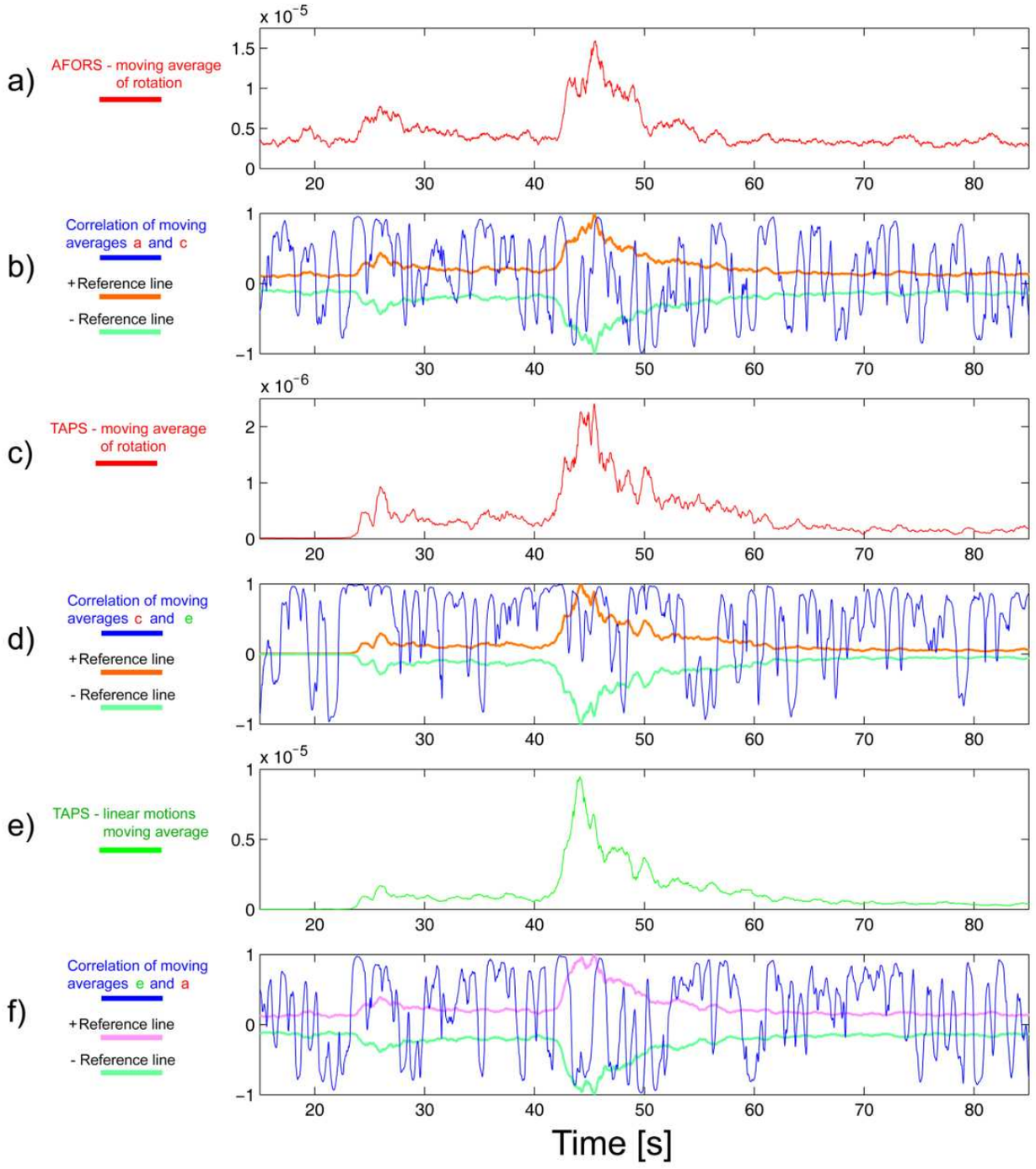


**Figure 17.** Relations of rotations and linear signals at the event in Jarocin area registered on January 6th, 2012. Diagrams descriptions as in Fig. 15

We did not find yet any other rules, especially – we did not find any relation between episodes of negative correlations (near -1) and the initial moving averages. We suppose that such comparison method may be useful in analysis of various chains, and especially their moving

averages, as in this work. Crucial point is that not the original signals, but chains of their absolute values are compared.

## 4. Conclusions

Simultaneous measurements of the rotations in seismic field with the use of completely different instruments – here AFORS-1 which is the Sagnac interferometer and the micro-array of TAPSs allow for comparison of the used equipment. In this work, such comparison revealed that signals differ significantly, to the degree which complicates analysis. From both kind of instruments, rotations are obtained in the same time-periods, but their plots differ. These differences are attributed partly to difference in instruments spectra and partly to disturbances in the signals, of technical provenience. Nevertheless, an analysis using the moving averages of absolute signals values, and consequently also coefficients of correlation between these averages confirmed common roots of these recorded signals, despite all their imperfections.

Research on seismic rotational effects, especially in buildings and other large constructions is widely recognized as very important and therefore these studies flourish. On the other hand, rotational components in the seismic field are also studied in various ways, but even existence of these components still evoke controversy. Presence of these components in seismograms, especially in their initial part which, according to classical theory of elasticity, contain only compressional waves, is explained in various ways. Authors believe that no one contemporary explanation is complete and proven, but this not preclude usefulness of further studies.

## Acknowledgements

This work was done in 2013-2014 under the financial support of the Polish Ministry of Science and Higher Education under Key Project POIG.01.03.01-14-016/08 “New photonic materials and their advanced application”, the MUT statutory activity PBS-850 and partially the the Polish National Centre for Research and Development under contract No PBS1/B3/7/2012.

## Author details

Anna Kurzych[1], Krzysztof P. Teisseyre[2], Zbigniew Krajewski[1] and Leszek R. Jaroszewicz[1*]

*Address all correspondence to: jarosz@wat.edu.pl

1 Institute of Applied Physics, Military University of Technology, Warsaw, Poland

2 Institute of Geophysics, Polish Academy of Sciences, Warsaw, Poland

## References

[1] Hobbs WH. Earthquakes. An Introduction to Seismic Geology. New York: Appleton and Co.; 1907.

[2] Davison Ch. The Founders of Seismology. Cambridge: Cambridge University Press; 1927.

[3] Ferrari G. Note on the Historical Rotation Seismographs. In: Teisseyre R., Takedo M., Majewski E. (eds) Earthquake Source Asymmetry, Structural Media and Rotation Effects. Berlin-Heidelberg-New York: Springer; 2006. p367-376.

[4] Kozak JT. Development of Earthquake Rotation Effect Study. In: Teisseyre R., Takedo M., Majewski E. (eds) Earthquake Source Asymmetry, Structural Media and Rotation Effects. Berlin-Heidelberg-New York: Springer; 2006. p3-10.

[5] Imamura A. Theoretical and Applied Seismology. Tokyo: Maruzen Co.;1937.

[6] Gutenberg B. Grundlagen der Erdbebrnkunde. Frankfurt: Univ. Frankfurt a/M; 1927.

[7] Teisseyre R. Earthquake Processes in a Micromorphic Continuum. Pure Applied Geophysics 1973; 102(1) 15-28.

[8] Teisseyre R. Symmetric Micromorphic Tin Space Continuum: Wave Propagation, Point Source Solutions and Some Applications to Earthquake Processes. In: Thoft-Christensen P. (ed.) Continuum Mechanics Aspects of Geodynamics and Rock Fracture Mechanics. Dodrecht-Boston: D. Reidel Publ. Comp.; 1974. p201-244.

[9] Eringen AC. Mirocontinuum Field Theories. Vol. 1 Foundations and Solids. New York: Springer-Verlag; 1999.

[10] Teisseyre R, Boratyński W. Continuum with Self-Rotation Fields: Evolution of Defect Fields and Equations of Motion. Acta Geophysica 2002; 50(3) 223-229.

[11] Teisseyre R. Asymmetric Continuum Mechanics: Deviations from Elasticity and Symmetry. Acta Geophysica 2005; 53(2) 115-126.

[12] Teisseyre R, Białecki M, Górski M. Degenerated Mechanics in a Homogeneous Continuum: Potentials for Spin and Twist. Acta Geophysica 2005; 53(3) 219-223.

[13] Teisseyre R, Górski M. Transport in Fracture Processes: Fragmentation of Defect Fields and Equations of Motion. Acta Geophysica 2009; 57(5) 583-599.

[14] Teisseyre R, Suchcicki J, Teisseyre KP, Wiszniowski J, Palangio P. Seismic Rotation Waves: Basic Elements of Theory and Recording. Annals of Geophysics 2003; 46(4) 671-685.

[15] Teisseyre R., Kozák JT. Sources of Rotation and Twist Motions. In: Teisseyre R, Takedo M., Majewski E. (eds) Earthquake Source Asymmetry, Structural Media and Rotation Effects. Berlin-Heidelberg-New York: Springer; 2006. p11-23.

[16] Teisseyre R, Takeo M, Majewski E. Earthquake Source Asymmetry, Structural Media and Rotation Effects. Berlin-Heidelberg-New York: Springer; 2006.

[17] Lee WHK, Cęlebi M, Todorovska MI, Igel H. (guest eds) Rotational Seismology and Engineering Applications. California: Bulletin of the Seismological Society of America 99(2B); 2009.

[18] Cowsik R, Madziwa-Nussinov T, Wagoner K, Wiens D, Wysession M. Performance Characteristics of a Rotational Seismometer for Near-Field and Engineering Applications. Bulletin of the Seismological Society of America 2009; 99(2B) 1181-1189.

[19] Droste Z, Teisseyre R. Rotational and Displacemental Components of Ground Motion as Deduced from Data of the Azimuth System of Seismograph. Publications od Institute of Geophysics Polish Academy of Science 1976; 97 157-167.

[20] Riedesel MA, Moore RD, Orcutt JA. Limits of Sensitivity of Inertial Seismometers and Velocity Transducer and Electronic Amplifiers. Bulletin of the Seismological Society of America 1990; 80 1725-1752.

[21] Teisseyre R, Nagahama H. Micro-Inertia Continuum: Rotations and Semi-Waves. Acta Geophysica Polonica 1999; 47 259–272.

[22] Jaroszewicz LR, Krajewski Z, Solarz L, Marc P, Kostrzyński T. A New Area of the Fiber-Optic Sagnac Interferometer Application. In: Proceedings of the 2003 SBMO/IEEE MTT-S International Conference on Microwave and Optoelectronics, 20–23 September 2003, Rio de Janeiro, Brazil, 2003.

[23] Sagnac G. L'éther lumineux démontré par l'effet du vent relative d'éther dans un interférométre en rotation uniforme. [in French] Comptes rendus de l'Académie des Sciences 1913; 95 708–710.

[24] Schreiber U, Schneider M, Rowe CH, Stedmanand GE, Schluter W. Aspects of Ring Lasers as Local Earth Rotation Sensors. Surveys in Geophysics 2001; 22 603–611.

[25] Jaroszewicz LR., Krajewski Z., Solarz L. Absolute Rotation Measurement Based on the Sagnac Effect. In: Teisseyre R., Takeo M., Majewski E. (eds) Earthquake Source Asymmetry, Structural Media and Rotation Effects. Berlin-Heidelberg-New York: Springer; 2006. p413–438.

[26] Takeo M, Ueda H, Matzuzawa T. Development of a High-Gain Rotational-Motion Seismograph. Grant 11354004. Earthquake Research Institute University of Tokyo; 2002. p5–29.

[27] Nigbor RL, Evans RJ, Hutt C. Laboratory and Field Testing of Commercial Rotational Seismometers. Bulletin of the Seismological Society of America 2009; 99, 1215–1227.

[28] Schreiber KU, Stedman GE, Igel H, Flaws A. Ring Laser Gyroscopes as Rotation Sensors for Seismic Wave Studies. In: Teisseyre R., Takeo M., Majewski E. (eds) Earth-

quake Source Asymmetry, Structural Media and Rotation Effects. Berlin-Heidelberg-New York: Springer; 2006. p377-390

[29] Kurzych A, Jaroszewicz LR, Krajewski Z, Teisseyre KP, Kowalski JK. Fibre Optic System for Monitoring Rotational Seismic Phenomena. Sensors 2014;14 5459-5469.

[30] Jaroszewicz LR, Krajewski Z, Teisseyre KP. Usefulness of AFORS - Autonomous Fibre-Optic Rotational Seismograph for Investigation of Rotational Phenomena. Journal of Seismology 2012; 16(4) 573-586.

[31] Teisseyre KP. Mining Tremors Registered at Ojców and Książ Observatories: Rotational Field Components, Publications of Institute Geophysics Polish Academy of Sciences 2006; M-29(395) 77-92.

[32] Teisseyre KP. Analysis of a Group of Seismic Events Using Rotational Components. Acta Geophysica 2007; 55(4) 535-553.

[33] Moriya T, Teisseyre R. Discussion on the Recording of Seismic Rotation Waves. Acta Geophysica Polonica 1999; 47 351-362.

[34] Teisseyre R, Suchcicki J, Teisseyre KP. Recording the Seismic Rotation Waves: Reliability Analysis. Acta Geophysica Polonica 2002; 51 37-50.

[35] Nowożyński K. Teisseyre KP. Time-Domain Filtering of Seismic Rotation Waves. Acta Geophysica Polonica 2003; 51 51-61.

[36] Solarz L, Krajewski Z, Jaroszewicz LR. Analysis of Seismic Rotation Detected by Two Antiparallel Seismometers: Spine Function Approximation of Rotation and Displacement Velocities. Acta Geophysica Polonica 2004; 52 198-217.

[37] Post EJ. Sagnac Effect. Review of Modern Physics 1967; 39(2) 475-493.

[38] Vali V, Shorthill RW. Fiber Ring Interferometer. Applied Optics 1976; 15(5) 1099-1100.

[39] Ulrich R. Fiber-Optic Rotation Sensing with Low Drift. Optics Letters 1980; 5(5) 173-175.

[40] Arditty H, Lefèvre HC. (1981). Sagnac Effect in a Fiber Gyroscope, Optics Letters 1981; 6(8) 401-403.

[41] Martin JM, Winkler JT. Fiber-Optic Laser Gyro Signal Detection and Processing Technique. SPIE Proceedings 1978; 139 98-102.

[42] Bergh RA, Lefèvre HC, Shaw HJ. All-Single-Mode Fiber-Optic Gyroscope with Long-Term Stability. Optics Letters 1981; 6(10) 502-504.

[43] Ezekiel S, Davis JL, Hellwarth RW. Intensity Dependent Nonreciprocal Phase Shift in a Fiber-Optic Gyroscope. Springer Series in Optical Sciences 1982; 32 332-336.

[44] Fredricks RJ, Ulrich R. Phase-Error Bounds of Fibre Gyro with Imperfect Polariser/ Depolarizer. Electronic Letters 1984; 20(8) 330-332.

[45] Lefèvre HC, Bettini JP, Vatoux S, Papuchon M. Progress in Optical Fiber Gyroscopes Using Integrated Optics. Proceedings of AGARD-NATO 1985; CPP-383 9A1-9A13.

[46] Burns WK. Phase-Error Bounds of Fiber Gyro With Polarization-Holding Fiber. Journal of Lightwave Technology 1986; LT4(1) 8-14.

[47] Lefèvre HC, Graindorge Ph, Arditty HJ, Vatoux S, Papuchon M. Double Closed-Loop Hybrid Fiber Gyroscope Using Digital Phase Ramp. Proceeding of OFS-3 1985, San Diego, OSA/IEEE, Postdeadline Paper 7

[48] Auch W. The Fiber-Optic Gyro – a Device for Laboratory Use Only?, SPIE Proceedings 1986; 719, 28-34.

[49] Arditty HJ, Graindorge Ph, Lefèvre HC, Martin Ph, Morisse J, Simonpiétri P. Fiber-Optic Gyroscope with All-Digital Processing. Proceedings of OFS- 6, Paris, Springer-Verlag Proceedings in Physics 1989; 44 131-136.

[50] Jaroszewicz LR, Krajewski Z, Kowalski H, Mazur G, Zinówko P, Kowalski JK. AFORS Autonomous Fibre-Optic Rotational Seismograph: Design and Application. Acta Geophysisica 2011; 59, 578–596.

[51] Jaroszewicz L.R., Krajewski Z., Teisseyre, K. P. The Possibility of a Continuous Monitoring of the Horizontal Buildings' Rotation by the Autonomous Fibre-Optic Rotational Seismograph AFORS Type. In: Lavan O., De Stefano M. (eds) Seismic Behaviour and Design of Irregular and Complex Civil Structures. Berlin-Heidelberg: Springer-Verlag; 2013. p339-351.

[52] Jaroszewicz LR, Krajewski Z. Application of the Fibre-Optic Rotational Seismometer in Investigation of the Seismic Rotational Waves. Opto-Electronics Review 2008; 16(3) 314-320.

[53] Böhm K, Marten P, Standigel L, Weidel E. Fiber-Optic Gyro with Digital Data Processing. 2nd International Conference on Optical Fiber Sensors, Stuttgart, Germany, 5–7 September 1984; 251–258.

[54] Krajewski Z. Fiber-Optic Sagnac Interferometer as System for Rotational Phenomena Investigation Connected with Seismic Events. (In Polish) PhD thesis, Military University of Technology, Warsaw; 2005.

[55] Krajewski Z, Jaroszewicz LR, Solarz L. Optimization of Fiber-Optic Sagnac Interferometer for Detection of Rotational Seismic Events. In Proceedings of SPIE 5952, Optical Fibers: Applications, Warsaw, Poland, 28 August–2 September 2005; 240–248.

[56] Dai X, Zhao X, Cai B, Yang G, Zhou K, Liu C. Quantitative Analysis of the Shupe Reduction in a Fiber Optic Sagnac Interferometer. Optical Engineering 2002; 41 1155–1156.